

Triborheology and Orientational Dynamics of Ionic Liquid Crystals

N. V. Pogodina*, T. Amann**, C. Dold**, E. Metwalli***, P. Müller-Buschbaum***, A. Kailer**, C. Friedrich*

*University of Freiburg, Freiburger Materialforschungszentrum-FMF, Laboratory of Experimental Rheology, Germany, Freiburg, Email: natalia.pogodina@fmf.uni-freiburg.de

**Fraunhofer Institute for Mechanics of Materials IWM, Germany, Freiburg, Email: tobias.amann@iwm.fraunhofer.de

***Technische Universität München, Physik-Department, Lehrstuhl für Funktionelle Materialien, James-Franck-Str. 1, 85748 Garching, Germany

Received**** 2013

Abstract

We present studies of triborheological properties and orientational dynamics of three imidazolium-based ionic liquids (ILs) [C14mim][BF₄], [C14mim][PF₆], [C14mim][Tf₂N], by utilizing a variety of physical methods including DSC, SAXS/WAXS, rheology, flow dichroism and tribology. Results revealed that two ILs ([C14mim][BF₄] and [C14mim][PF₆]), which possess a liquid crystalline (LC) phase show ultralow friction and lower wear as poly-alpha-olefin (PAO) standard lubricant oil in the isotropic phase at 120°C. Moreover, the [C14mim][BF₄] IL exhibits also ultralow coefficient of friction (COF) in its LC phase. Such unique tribological behavior originates from bilayered domain structure, which is maintained by the specific molecular interactions and orientation in the shear flow. SAXS data revealed that cation tails in LC domains are interdigitated in a bilayer smectic phase. In strong shear flows LC domains tend to be oriented along the flow direction which is confirmed by sigmoidal growth of flow dichroism values. The dichroism signal does not relax even when the flow is stopped due to long-range orientational order in LC domains. The negative sign of the dichroism indicates orientation of anisotropic mobile cation tails perpendicular to the flow directions. This specific bilayered domain structure is well pronounced in LC phase and the “precursors” of these domains exist also in the isotropic phase, giving rise to ultralow friction regime in sliding contacts.

Keywords: Ionic Liquid Crystals; triborheology; friction and wear; orientational dynamics

1. Introduction

Energy dissipation due to friction and wear are significant economic factors which have to be minimized to increase the energy efficiency of technical systems. Especially in terms of energy efficiency standard mineral-based lubricants are limited in a particular area and must be enriched by different additives such as friction modifiers or extreme pressure additives. Therefore novel lubricants with specific physical properties are sought to realize strongly low friction losses. A certain area of the current research focuses on ionic liquids (ILs) because these fluids are promising lubricants [1], [2] due to their specific physical properties and opportunities for possible applications [3], [4]. The number of publications concerning the tribology of ionic liquids rises steadily per year, which reflects the potential of this class of fluids as lubricants. Some publication describe that imidazolium-based ILs may act like a classical friction modifier to reduce

friction in tribological contacts [2], [5], [6].

Our own studies of ILs confirmed that ILs are complex fluids formed by heterogeneous polar and nonpolar domains, which show structure formation in their liquid phase [7], [8]. The degree of structuring depends on chemical structure and type and strength of interactions (ionic, H-bonding, dipole-dipole, pi-pi). At high level of structuring we monitored even temporal network formation [8]. These different types of interactions are the dominant factors which determine the structuring process and physical properties of ILs. Our investigations also showed [9], [10], [11] [12], [13] that ILs exhibit improved tribological properties. However ILs, especially imidazolium-based ionic liquids, are extremely hygroscopic [14] but the quantity of adsorbed water decreases with increasing alkyl chain length [15]. ILs are prone to chemical reactions with steel, which lead to an increase of friction due to tribocorrosion [1], [16].

Ionic liquid crystals (ILCs) which combine the physical properties of liquid crystals and ionic liquids offer a great potential for applications which originates from their specific interactions. These multiple interactions support and stabilize lamellar mesophases and provide unique anisotropic electric, magnetic, optical and mechanical properties [17]. These fluids are able to form liquid crystalline mesophases within a specific temperature range. A recent overview of thermotropic ILCs and their properties was published by Axenov and Laschat [18]. Despite intensive research the triborheological behavior of ILCs is not fully understood and their full potential is not yet explored. Our own previous investigations of liquid crystal fluids not on the basis of ILCs [19], [20], [21], [22], and on the basis of ILC[C12mim][PF6] [9] have shown that these fluids exhibit ultralow friction values ($\mu \approx 0.005 - 0.01$). ILCs show specific non-Newtonian rheological behavior especially in the liquid crystalline phase [9], [23]. In some publication ILs were successfully used as oil additives [24], [25], [26], [27], [28], [29], [30] and as diesel additive [31] to improve the tribological performance.

This promising tribological behavior of ILCs originates from their chemical structure, interactions and molecular orientation under shear. However it is not yet understood how the ILC molecules are oriented, how this molecular orientation can be influenced and controlled by the shear flow and which orientational state leads to the superlow friction.

Here we study triborheological properties and orientational dynamics of 3 imidazolium-based ILs with different anion structure ([C14mim][BF4], [C14mim][PF6], [C14mim][Tf2N]), with the aim to understand and quantify their orientational behavior in anisotropic and isotropic phases and to correlate it with their chemical structure, friction and wear properties.

The distinguished characteristics of liquid crystalline state of ILC is the tendency of the molecules to point along a director which leads to anisotropic interaction with light and to anisotropic optical properties like birefringence and dichroism.

We utilize a variety of physical methods including differential scanning calorimetry (DSC), small- and wide- angle X-ray scattering (SAXS/WAXS), rheology, flow dichroism, tribology. Wear and corrosivity were analyzed using optical measurements and energy dispersive X-ray spectroscopy. The studies have been carried out on pure ILs as well as on their mixtures with poly-alpha-olefins in LC and isotropic phases.

2. Experimental

2.1. Materials

Three imidazolium-based ([C14mim]; Fig.1a) salts have been used with three different anions (Fig.1b-c). The two ILs containing hexafluorophosphate [PF6] and tetrafluoroborate [BF4] anions are thermotropic ionic liquid crystals (ILCs), because they are able to form a liquid crystalline phase in a specific temperature range. In contrast, the third IL with bis(trifluoromethylsulfonyl)imide [Tf2N] anion possess no LC phase. The alkyl chain of the imidazolium-based cation consists of 14 carbon atoms and should therefore be mixable with a standard-oil, which is also nonpolar. Therefore poly-alpha-olefin (PAO, 30 mPa·s at 100 °C) was used as a reference oil and for the mixtures. To evaluate the miscibility of the [C14mim] containing substances with PAO oil we also studied lubricating properties of the [C2mim][PF6] IL, with a very short alkyl chain, mixed with PAO oil. Due to the different anions the ionic liquids have different molecular weight and different amount of absorbed water (Tab.1). All employed experimental methods are explained in the ESI.

Table 1. Water content and molecular weight of the used ionic liquids.

Ionic Liquid	Water content ^a (ppm)	Molecular weight (g/mol)
[C14mim][PF6]	651	424.45
[C14mim][BF4]	1325	366.29
[C14mim][Tf2N]	176	599.64

a. manufacturer information from Iolitec GmbH.

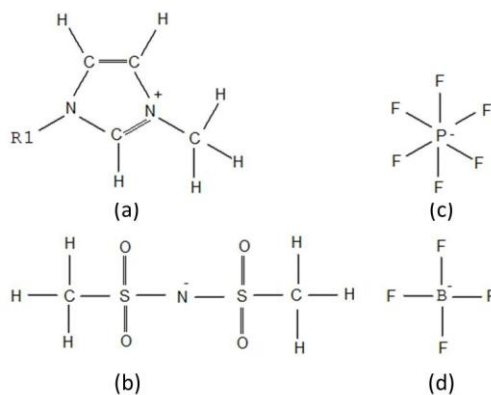


Figure 1. Chemical basic structure of the used various ions: a) Methyl-Imidazolium [C(R)mim] cation with variable alkyl chain length R; b) Bis(trifluoromethylsulfonyl)imide [Tf2N]; c) Hexafluorophosphate [PF6]; d) Tetrafluoroborate [BF4].

3. Results and Discussion

3.1. Phase Transition Temperatures

The phase transition temperatures have been determined by DSC (Fig.2) and rheology (Fig.3). Fig. 2 shows comparative DSC second heating scans of the three studied ILs with a heating rate of 2K/min. The [C14mim][BF4] and [C14mim][PF6] showed two distinct phase transition peaks: crystalline (C) – liquid-crystalline (LC) and LC-isotropic. The [C14mim][Tf2N] shows only one C-isotropic transition peak.

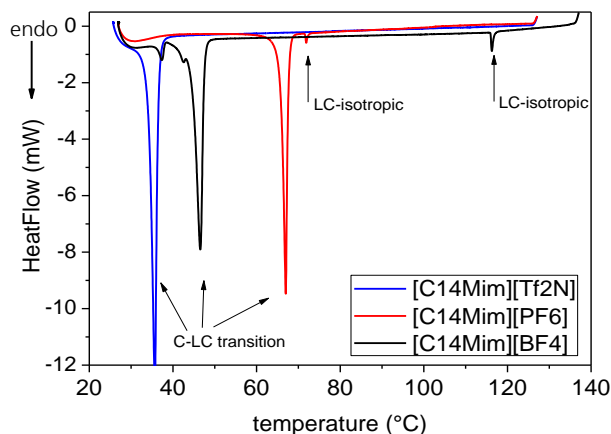


Figure 2. DSC second heating scans (2K/min) for the three studied ILs identified in the inset. C-LC, LC-isotropic and C-isotropic transition peaks are marked by the arrows.

Comparative rheological heating ramps of the three ILs with the same heating rate of 2K/min (Fig.3) confirm two transitions C-LC and LC-isotropic for [C14mim][BF4] and [C14mim][PF6]. Each transition is manifested in the sharp decrease of complex viscosity by several orders of magnitude. [C14mim][BF4] has a wide temperature range of LC phase (50–115°C), while [C14mim][PF6] has a narrow temperature range of mesophase (67–72°C). [C14mim][Tf2N] shows only one C – isotropic phase transition at 36°C when the viscosity drops by 4 orders of magnitude and exhibits Newtonian flow behavior in the whole temperature range.

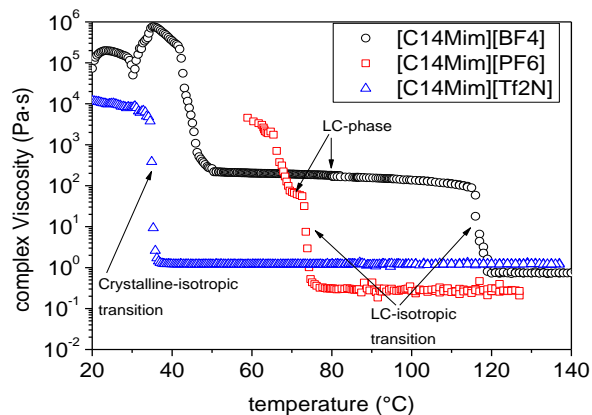


Figure 3. Complex viscosity versus temperature during heating ramps (2K/min) for the three studied ILs identified in the inset. C-LC and LC-isotropic transitions are marked by the arrows.

The temperatures at which the viscosity jumps occur, agree well with the transition temperatures from DSC and are given in the Table 3 together with the transformation enthalpies and viscosities in LC and isotropic phases (ESI). Two temperatures have been chosen for the following studies: 70°C in LC phase and 120°C in isotropic phase.

3.2. Structural Studies by SAXS/WAXS

The structure of [C14mim][Tf2N], [C14mim][BF4], and [C14mim][PF6] ILs has been probed using WAXS and SAXS

techniques (Figs. 4, 5).

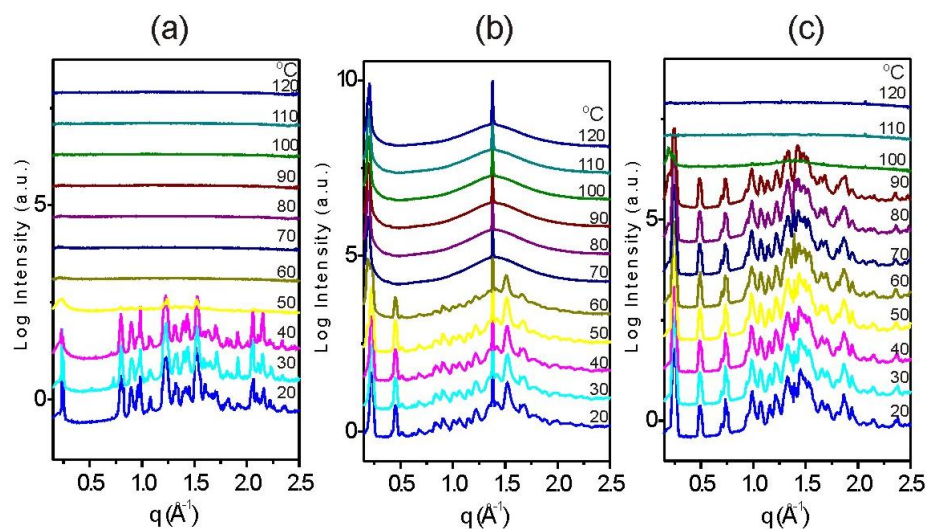


Figure 4. WAXS profiles of a) [C14mim][Tf2N], b) [C14mim][BF4], c) [C14mim][PF6] ILs at different temperatures from 20°C up to 120°C in 10°C steps (from bottom to top) at a heating rate of 5°C/min. The temperature is stabilized for 10 min at each temperature before the 20 min data acquisition.

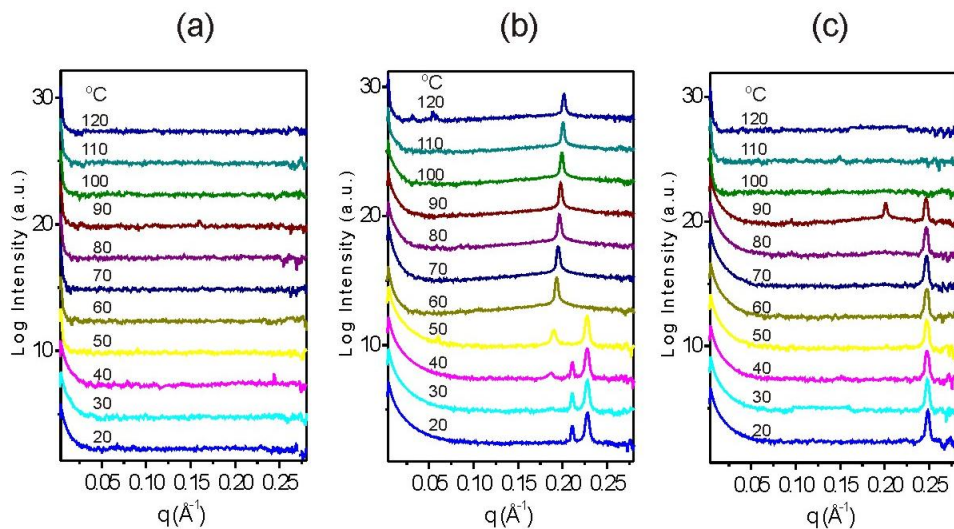


Figure 5 SAXS profiles of a) [C14mim][Tf2N], b) [C14mim][BF4], c) [C14mim][PF6] ILs at different temperatures from 20°C up to 120°C in 10°C steps (from bottom to top) at a heating rate of 5°C/min. The temperature is stabilized for 10 min at each temperature before the 30 min data acquisition.

Figure 4 shows the WAXS profiles for the three studied ILs upon heating which reveal phase transitions at 50 °C, 70 °C and 100 °C for [C14mim][Tf2N], [C14mim][BF4], and [C14mim][PF6] ILs, respectively. These phase transitions are comparable to those observed by DSC (Figure 2) and by rheology (Fig.3), which show major transitions for all the

samples. The transition temperatures observed by the WAXS measurements are relatively higher than those observed by DSC and rheology. This may be attributed to different thermal history employed in three techniques. For WAXS measurements, a total time of about 10 min at each temperature is used for thermal stabilization. Without a prior thermal treatment of the samples the data acquisition at a heating rate of 5°C/min is acquired. The structural evolution of the materials is clearly seen on the temperature dependent WAXS profiles (Figure 4). For all ILs, there are multiple diffraction peaks at q range from 0.15 - 2.5 Å⁻¹ (Figure 4) indicating well-structured 3D crystalline compounds [32], [33]. As the temperature increases and melting occurs, all the characteristic crystalline structural peaks suddenly disappear. A crystalline peak at 1.37 Å⁻¹ in Fig. 4b is due to the mica windows used to sandwich the ILs material.

To probe possible large size structures, the SAXS data have been collected. Figure 5 shows the SAXS profiles for the three studied ILs upon heating in the temperature range 20 – 120°C. There is a distinctive structural difference in the phase transition behavior from all investigated materials. The phase transitions for the [C14mim][Tf2N] IL can be assigned as a transition from solid crystals to isotropic liquid as revealed by the absence of any characteristic peaks at low q values upon heating (Figure 5a). In contrast to this, for the [C14mim][BF4], a new scattering peak at low q = 0.190 Å⁻¹ associated with LC phase (Figure 5b) initially appears at 50°C and pertains till high temperatures up to 120°C. This peak systematically shifts from 0.190 Å⁻¹ to 0.201 Å⁻¹ with increasing temperature from 50°C to 120°C and represents the layer spacing of the [C14mim][BF4] IL in the LC phase. According to Tanford [34] the distance from the imidazolium ring to the periphery of carbon chain (l_{cat}) can be estimated from the equation; $l_{cat}(\text{Å}) = 1.5 + 1.265N$, where N is the number of carbon in the tail. From the latter equation, the l_{cat} for the [C14mim][BF4] IL is 21.74 Å and due to possible carbon tail interdigitation the layer thickness (D) is $l_{cat} < D < 2l_{cat}$. The experimental D value (33.1 Å) at 50°C reveals that the carbon chains are interdigitated ($2 l_{cat} = 43.48 \text{Å}$) in the bilayer assembly which suggests a smectic phase (see further Fig.13). The layer spacing of [C14mim][BF4] LC phase decreases from 33.1 to 31.3 Å with increasing the temperatures from 50°C to 120°C. At high temperatures, the chain tails occupy more free space due to an increase of both the chain motion and the chain conformational disorder resulting in a high degree of interdigitation and hence a decrease of the layer spacing. This temperature dependence of the layer spacing D is consistent with those reported in [35] for the [C16mim][Br] IL crystalline phases. It is important to emphasize that even at high temperature of 120°C there exists a distinct structural peak at low scattering vector $q = 0.201 \text{ Å}^{-1}$ (Fig 5b) that confirms ordered and layered structural organization of the [C14mim][BF4], which leads to “sliding” mechanism and improved tribological performance in high shear flow observed at 120°C (further sections) The crystalline structure of the [C14mim][BF4] IL at low temperatures (20-40°C) is revealed in the WAXS multi peaks reflections (Figure 4b) and in the SAXS profiles (Figure 5b). The latter show two additional peaks at 0.227 Å⁻¹ and 0.211 Å⁻¹ which correspond to $D = 27.7 \text{ Å}$ and $D = 29.8 \text{ Å}$ and indicate a very high interdigitation of the carbon chain tails in the crystalline phase of [C14mim][BF4] IL.

Figure 5c shows the SAXS profiles of the [C14mim][PF6] IL at different temperatures. A reflection peak at 0.248 that pertains from 20°C up to 90°C and an additional new peak at 0.201 Å⁻¹ appears at 90°C. Both peaks vanish at temperatures around 100°C. These results show that the formation of smectic liquid crystal phase in [C14mim][PF6] with layer spacing of 31.3 Å occurs only at a high temperature of 90°C and this LC phase coexists with the crystalline phase ($D = 25.3 \text{ Å}$), so that a solid-like behavior in LC temperature range may be present. The temperature range of LC smectic phase is narrow, since crystalline/liquid crystal to isotropic transition occurs already at lower (than for the

[C14mim][BF4]) temperature of 100°C.

3.3. Viscoelastic properties (SAOS)

Fig.6 shows stress sweep for [C14mim][BF4] and [C14mim][PF6] in the LC state. Dynamic moduli and complex viscosity are independent of shear stress at low stresses, indicating linear viscoelastic region. Storage modulus exceeds loss modulus since in LC phase ILs exist in the “gel-like” state. At the critical shear stress of 10Pa for [C14mim][BF4] and 4Pa for [C14mim][PF6] (indicated by the arrows in Fig.6) materials start to flow (the structural order is destroyed) and at even higher stresses crossover occurs, where loss modulus takes over storage modulus. At the same temperature of 70°C the gel of [C14mim][BF4] possess ten times higher elasticity and viscosity than gel of [C14mim][PF6], which may indicate higher order of LC domains in this IL.

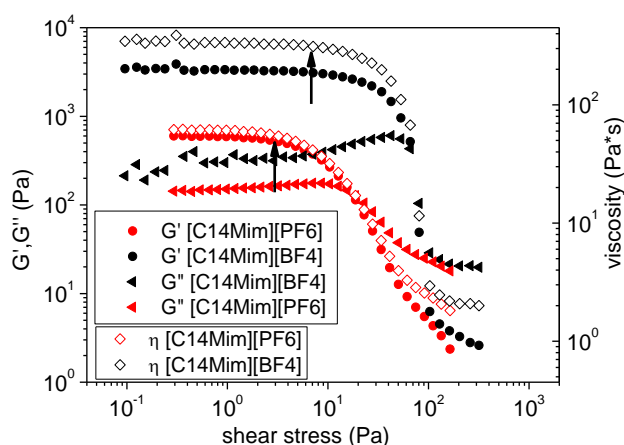


Figure 6. Evolution of dynamic moduli (left axis) and complex viscosity (right axis) during stress sweep at 70°C for the two ILs identified in the inset. The critical shear stress when LC gels start to flow is marked by the arrows.

Frequency sweeps (Fig.7) show viscoelastic properties for all 3 ILs at 70°C. In the whole probed frequency range storage modulus exceeds loss modulus $G' > G''$ and a power law dependence of viscosity (strong shear-thinning) is observed for [C14mim][BF4] and [C14mim][PF6], which is a typical gel behavior in the mesophase. In contrast to this the [C14mim][Tf2N] IL exhibits very low Newtonian viscosity (no shear thinning effect in the probed frequency range) typical for isotropic molecular fluid.

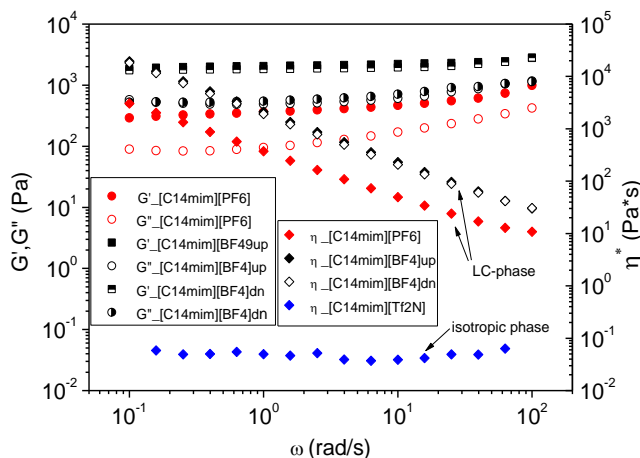


Figure 7. Evolution of dynamic moduli (left axis, circles and squares) and complex viscosity (right axis, diamonds) during frequency sweep at 70°C for the three ILs identified in the inset.

3.4. Flow curves (steady mode)

The flow behavior was studied in LC and isotropic phases in a very broad shear rate range of 7 decades (Fig.8). Flow curves were monitored at the increasing shear rates (up) followed by the decreasing shear rates (down) and showed reversibility (no thixotropic effect). In LC state strong reversible shear thinning was observed for the two ILCs at 70°C. This shear-thinning behavior has 3 regions (identified from high shear rates (region I) to low shear rates (region III)): (I)- high-shear rate shear-thinning regime, followed by (II) intermediate plateau, followed by (III) low-shear rate shear-thinning region. Viscosity flow curves for our ILs resemble shear viscosity curve of Onogi and Asada [36] for main-chain liquid-crystalline polymers (LCP). Regions I and II are common for the isotropic fluids and polymers, but not the region III. Thus the most distinguishing feature of LC-phase is the observed additional low-shear-rates shear thinning regime III. In the isotropic state all three ILs show at high shear rates extended Newtonian flow behavior with viscosity values below 0.1 Pa·s (Fig.8, Table 3 (ESI)).

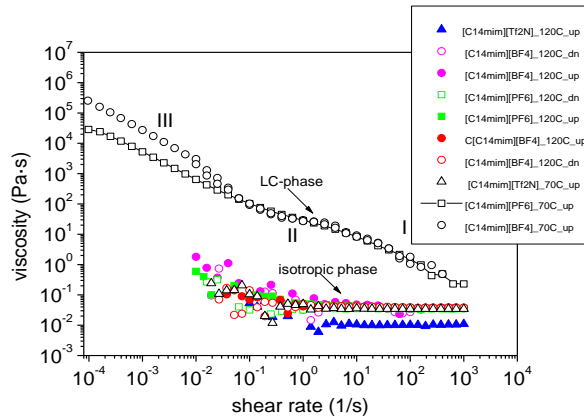


Figure 8. Viscosity versus shear rate for 3 ILs identified in the inset at 70°C and 120°C. Shear rate sweep is taken with increasing (up) and with decreasing (dn) shear rates.

3.5. Orientational Dynamics by Flow Dichroism

Dichroism refers to the tendency of anisotropic materials to preferentially absorb light that is polarized in certain directions. Dichroism is linked to the imaginary part of the refractive index tensor n''_{ij} and is defined as

$$\Delta n'' = n''_1 - n''_2. \quad (1)$$

Here n''_1 and n''_2 are the principal values of the refractive tensor. The dichroism $\Delta n''$, is recovered from the extinction

$$\delta'' = 2\pi\Delta n''d/l \quad (2)$$

where d is the thickness of the sample (gap of the rheometer plates) [37], [38].

The applied shear rate protocol and the corresponding dynamic viscosities for the [C14mim][BF4] and [C14mim][Tf2N] at 70°C are shown in Fig. 9 and the flow dichroism versus time for both ILs is presented in Fig.10.

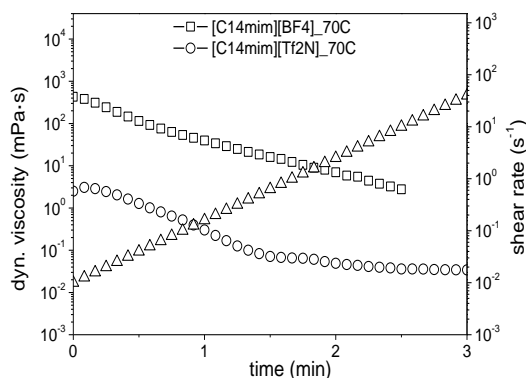


Figure 9. Shear rate protocol (right axis, triangles) and dynamic viscosity (left axis, squares and circles) at 70°C for the two ILs identified in the inset. Corresponding optical response is in Fig.10.

The shear rate protocol was applied when shear flow was increased continuously starting from shear rate $d\gamma/dt = 0.01 \text{ s}^{-1}$ up to $d\gamma/dt = 40 \text{ s}^{-1}$ (Fig.9) for 3 minutes. After that the flow was stopped and free relaxation of orientation was monitored optically. At low shear rates the magnitude of dichroism is small due to the dominance of Brownian motion. The distribution of orientations of ILC domains is close to isotropic. The corresponding average orientation angle of ILC domains is about 45° .

When the shear rate is increased, the hydrodynamic forces become dominant and ILC domains tend to orient closer to the flow direction. The corresponding average orientation angle is decreasing and at high shear rates (strong flow) reaches the value of $\sim 10^\circ$, while the magnitude of dichroism also shows sharp sigmoidal growth reaching the value of $\Delta n'' = -2 \cdot 10^{-4}$. The most fascinating fact is that the dichroism signal does not relax and stays constant at the same maximum value even when the flow is arrested after 3 minutes of shear. This is a specific behavior of C14MimBF4 domains in LC phase, which is characterized by long range orientational order that persists (monitored for extra 10 minutes in Fig.10) and prevents relaxation after the flow is stopped.

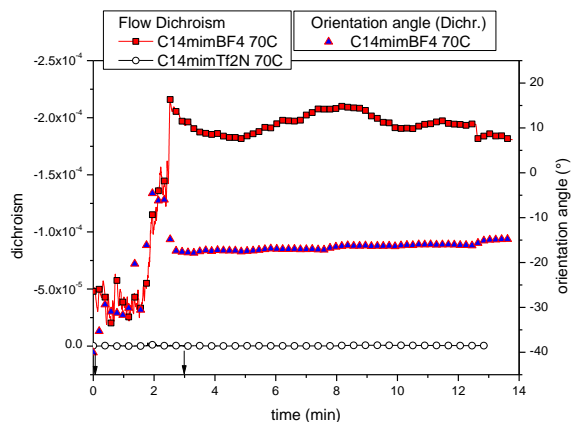


Figure 10 Dichroism (left axis, squares and circles) and orientation angle (right axis, triangles) versus time for the two ILs identified in the inset during shearing time of 3 minutes (marked by the arrows) followed by 10 minutes of free relaxation without shear

In sharp contrast to this behavior the [C14mim][Tf2N] shows no dichroism in the probed shear rate range (Fig.10) that

confirms the absence of intrinsic order and isotropic state of this IL.

The next applied shear protocol together with flow curves is shown in Fig.11 and the corresponding optical response is presented in Fig. 13. The same two ILs have been sheared for the total time of 6 minutes at first at a constant low shear rate of 0.1 s^{-1} for two minutes, followed by high shear rate of 100 s^{-1} for the next two minutes and again by low shear rate 0.1 s^{-1} for the last 2 minutes.

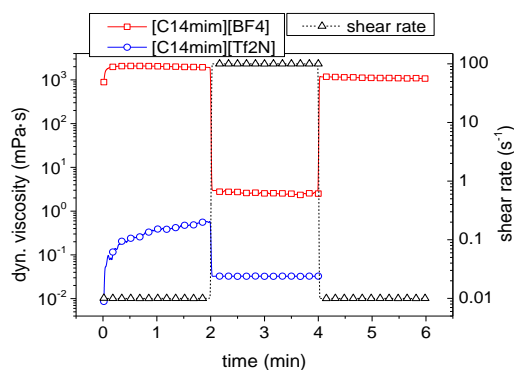


Figure 11. Shear rate protocol (right axis, triangles) and dynamic viscosity (left axis, circles and squares) for the two ILs identified in the inset. Corresponding optical response is in Fig.12.

Fig.11 demonstrates the strong effect of the flow on the shear viscosity of ILC [C14mim][BF4]. When the flow shear rate increases by 4 orders the viscosity drops by 3 orders of magnitude. Such dramatic decrease of dynamic viscosity is the result of alignment of LC domains in strong flows. This alignment and layering decreases the frictional resistance experienced by the neighboring LC domains and allows them more easily “slide” past one another. In contrast to this the viscosity of [C14mim][Tf2N] in isotropic state is low from the very beginning and does not experience such dramatic decrease in high shear flow, since the mechanism of “sliding” is absent. Optical response in [C14mim][BF4] (Fig.12) revealed again sharp sigmoidal growth of flow dichroism up to the final value of $-2.3 \cdot 10^{-4}$ which persisted after the flow was stopped (monitoring was continued for the next 14 minutes after the flow was arrested).

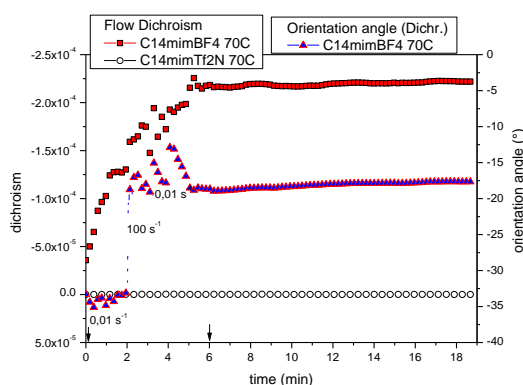


Figure 12. Dichroism (left axis, circles and squares) and orientation angle (right axis, triangles) versus time for the two ILs identified in the inset during shear flow of different intensities (total shearing time of 6 min marked by the arrows), followed by 14 minutes of free relaxation without shear.

This high dichroism value is a result of strong alignment of LC domains, which is also confirmed by a corresponding

decrease in orientation angle from 35° (at the flow start up) to 10° (end of the flow) and to 17° (without flow). The negative sign of the flow dichroism may be interpreted as sensing the anisotropy of structures that exhibit higher polarization perpendicular to the flow. In another words, the negative sign of the optical anisotropy may indicate local orientation of mobile anisotropic side groups of the cations (inside the flow aligned and ordered domains) perpendicular to the flow (Fig.13). There was again zero dichroism monitored for the isotropic IL [C14mim][Tf2N] (Fig.12).

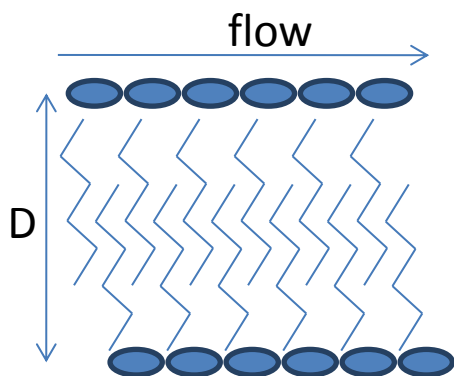
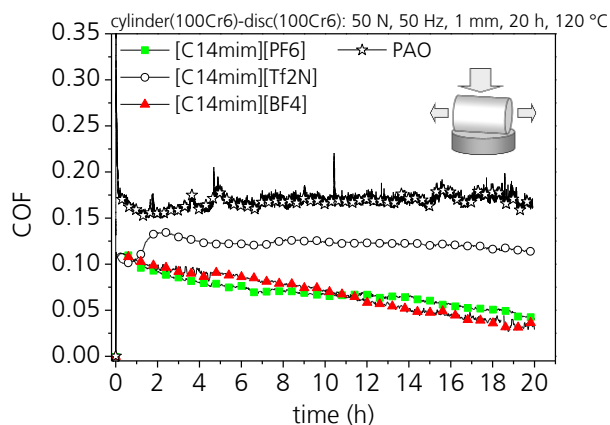


Figure 13. Schematic diagram of possible self-assembly in LC domains and their orientation in the flow field. Solid ellipsoids represent interacting polar heads of the imidazolium cation and $[\text{BF}_4]^-$ anion. Zig-zag rodlike C14 side chains (tails) are interdigitated forming a bilayer smectic phase. Anisotropic tails are oriented perpendicular to the flow direction. D is layer spacing.

Thus measurements of dichroism is a direct and effective way to detect existence of LC phase and to study orientational dynamics of LC domains.

3.6. Tribological behavior

The tribological behavior was studied in isotropic (120°C , fig.14a) and liquid crystalline phases (70°C , fig.14b) using cylinder-on-disc-geometry.



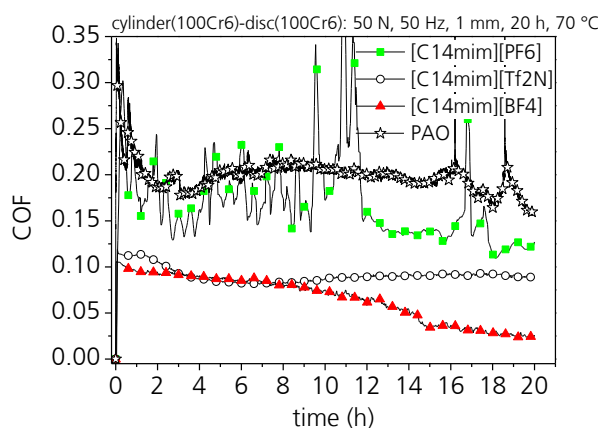


Figure 14. Tribological tests using cylinder-on-disc-geometry at (50 N, 1 mm, 50 Hz, 10 h): a) 120 °C; b) 70 °C.

Fig.14a shows that at 120 °C PAO has the highest COF ($\mu \approx 0.17$) of all tested fluids. In contrast to the [C14mim][Tf2N], which exhibits a constant COF of 0.09 during the whole testing time, the [C14mim][BF4] and the [C14mim][PF6] show a decrease of the COF with increasing testing time in the isotropic phase at 120°C. . After 20 h the COF is reduced to $\mu \approx 0.04$ for both LC fluids, which corresponds to less than 50% of their initial COF.

In the LC phase at 70°C (Fig. 14b) the [C14mim][BF4] shows also a decrease of COF to values as low as 0.02. This very low COF for the [C14mim][BF4] is observed despite two decades higher viscosity which this IL possess in LC phase (Table 3, ESI). Thus, low COF of [C14mim][BF4] in both states (isotropic and anisotropic) does not originate from low viscosity, but is rather governed by the “sliding” mechanism. This “sliding” is determined by bilayered structure and specific molecular orientation of [C14mim][BF4] cations side groups in shear flow. In the anisotropic state (70°C) it is a specific orientation of LC domains (studied by SAXS and dichroism in previous sections), which persists and provides “sliding” mechanism in shear flow. At 120°C LC domains may not exist, but specific orientational order and alignment of chemical groups as “precursors” of LC domains are present (as it is confirmed by SAXS peak at 120°C in Fig.5b) and maintain “sliding” mechanism in tribological behavior.

At 70°C the [C14mim][Tf2N], which has no mesophase, shows a constant COF of 0.11 during the whole testing time (Fig. 14b). The [C14mim][PF6] has a very unstable tribological behavior due to a narrow temperature range of mesophase around 70 °C and possible solid properties at this condition cannot be excluded (see also SAXS section Fig.5c)

Fig.15 illustrates the tribological behavior of pure PAO and mixtures of PAO with 1% of the ionic liquids. At the beginning of the test the COF can be reduced by adding 1% of an ILC, and the [C14mim][PF6] additive shows the lowest COF. However after approximately 15 min the COF increases to the same value ($\mu \approx 0.18$) as for the pure PAO. The [C2mim][PF6] was not mixable with PAO and so it has no effect and shows the same tribological behavior as pure PAO.

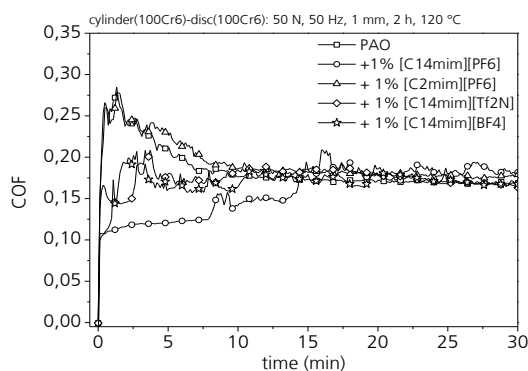


Figure 15. Tribological tests using cylinder-on-disc-geometry with pure PAO and mixtures of PAO with 1% of the ionic liquids (50 N, 1 mm, 50 Hz, 10 h, 120 °C).

3.7. Wear analysis

After the tribological tests the worn area of the cylinder was analyzed (fig.16) and the topology (fig.17) and roughness (ESI) of the wear scar surface was measured. As shown in fig.16a PAO causes the biggest worn area at 70 °C and 120 °C, except [C14mim][PF6] at 70 °C which results in the high amount of mixed lubrication due to the small temperature range of mesogenic phase. The worn area of the cylinder decreases from 120 °C to 70 °C for PAO and [C14mim][BF4] due to the increasing viscosity. The wear area for the [C14mim][Tf2N] does not change with temperature. The wear area of the cylinder using PAO and mixtures of PAO and ILCs is shown in fig.14b. There is a slight decrease of the wear area using [C14mim][BF4] and [C14mim][PF6].

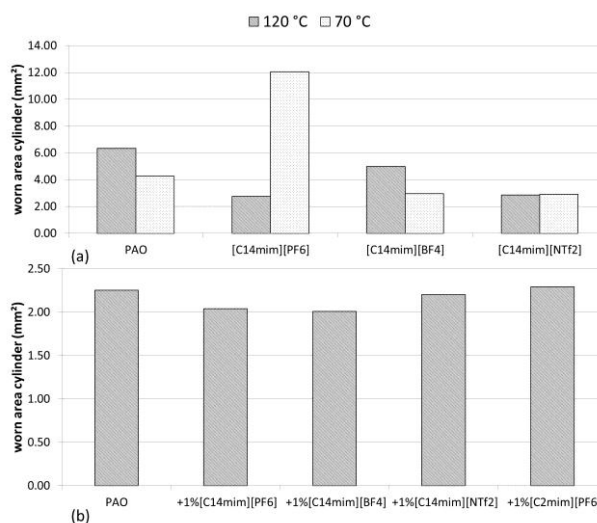


Figure 16. Wear area of the cylinder: a) pure fluids after 20 h testing time at 120 °C and 70 °C; b) pure PAO and mixtures with ILCs after 2 h testing time at 120 °C.

Using white light interferometry (WLI) the topology of the wear scar was measured after the tribological test. As illustrated in fig.17a,d by lubricating with PAO and mixtures of PAO with ILCs the surface is very rough and there are wear grooves along the sliding direction. In contrast using [C14mim][BF4] and [C14mim][PF6] a very smooth surface

is observed after test whereat with [C14mim][PF6] also wear grooves are formed. The roughness of the wear scars is higher at 70 °C as at 120 °C (fig.1 in ESI) and the highest Ra-values are found for PAO (approximately 5-times higher as with ILCs). This indicates that PAO has high adhesive wear in the mixed lubrication regime in contrast to the ionic substances, and this situation cannot be improved by adding only 1% ILC.

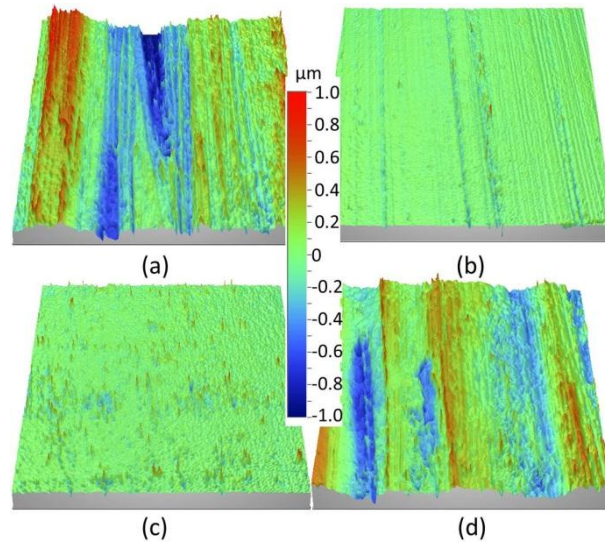


Figure 17. Wear scar analysis using white light interferometry (118.5x90.1 μm): a) PAO, 20 h, 120 °C; b) [C14mim][PF6], 20 h, 120 °C; c) [C14mim][Tf2N], 20 h, 120 °C; d) PAO+1% [C14mim][PF6], 2 h, 120 °C.

SEM images of the wear scars are shown in fig.18. In accordance with the WLI results fig.18a,d illustrates the adhesive wear of PAO and PAO mixture with [C14mim][PF6]. Only [C14mim][PF6] has a homogeneous surface and in contrast the surface after using [C14mim][Tf2N] shows some deposit. Further surface analytic using EDS shows that the neat surface of the wear scars has nearly the same amount of C, Fe and Cr (ESI tab.2). Using [C14mim][PF6] and [C14mim][Tf2N] a little amount of Si was detected on the surface and with [C14mim][PF6] some phosphorus (0.32%). Analyzing the deposit on the wear scar of [C14mim][Tf2N] also sulfur and oxide was detected at some areas which is an indication of corrosion processes.

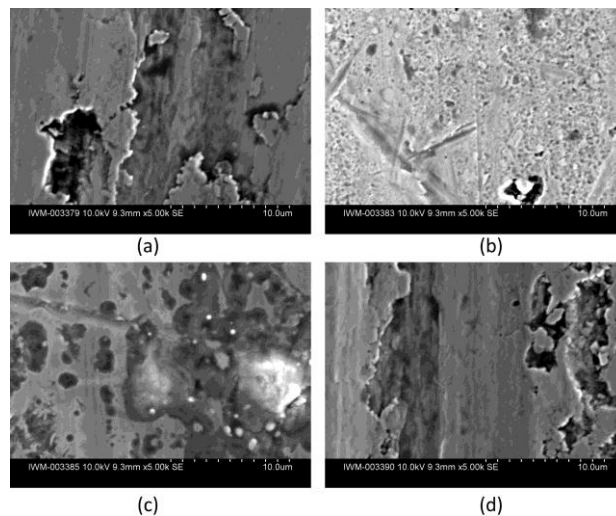


Figure 18.Wear scar analysis using SEM/EDS: a) PAO, 20 h, 120 °C; b) [C14mim][PF6], 20 h, 120 °C; c) [C14mim][Tf2N], 20 h, 120 °C; d) PAO+1% [C14mim][PF6], 2 h, 120 °C.

4. Conclusions

This research has been undertaken to explore triborheological properties and orientational dynamics of three imidazolium-based [C14mim] ILs with different anions [BF4], [PF6], [NTf2] in anisotropic and isotropic phases and to correlate it with their chemical structure. The studies have been carried out with the variety of complementary physical methods including DSC, SAXS and WAXS, rheology, flow dichroism and tribology. Friction and wear properties have been studied on pure ILs as well as on their mixtures with PAO.

Phase transition temperatures, determined by DSC and rheology, showed good agreement. [C14mim][BF4] and [C14mim][PF6] ionic liquids exhibit LC phase and two phase transitions, while [C14mim][Tf2N] possess no mesophase and has only one crystalline – isotropic transition. The LC temperature range of [C14mim][BF4] is wide in comparison with a very narrow LC T-range of [C14mim][PF6]. This wide, stable and well pronounced mesophase determines unique physical properties of [C14mim][BF4].

WAXS revealed multipeaks which indicate well-structured crystalline phases in all studied ILs at low temperatures.. For the [C14mim][BF4] a structural peak at low q-values has been detected by SAXS starting from 50°C, which is associated with LC phase and which shows a continuous shift with temperature increase. The corresponding value of layer spacing reveals interdigitation of the cation tails in the bilayer assembly, which suggests a smectic mesophase. This structural (smectic phase) peak exists even at 120°C, that confirms ordered and layered structural organization in [C14mim][BF4] responsible for the “sliding” mechanism and ultralow friction in anisotropic and isotropic phases.

Rheological studies showed that two ILs [C14mim][BF4] and [C14mim][PF6] exist in their mesophases in the state of gel, which is evidenced by $G' > G''$ and by low-shear rate shear-thinning region in the flow curves.

Flow dichroism was measured in the flows of different intensities and in the arrested flows. In the strong flows LC domains tend to orient along the flow direction and the dichroism shows sigmoidal growth reaching the plateau value of $\Delta n'' = - 2 \cdot 10^{-4}$. The most fascinating fact is that the dichroism signal does not relax and stays constant at the same maximum value even when the flow is arrested. This is a specific behavior of [C14mim][BF4] domains in LC phase which is characterized by a long range orientational order that persists, prevents relaxation after the flow is stopped and provides “sliding” and ultralow friction. The negative sign of the dichroism indicates local orientation of anisotropic cation tails perpendicular to the flow direction.

The [C14mim][BF4] and [C14mim][PF6] both show ultralow friction and lower wear as PAO in the isotropic phase at 120°C. The [C14mim][BF4] exhibits also ultralow COF in the LC phase although it has two orders higher viscosity in the mesophase. This last result suggests that ultralow COF of [C14mim][BF4] does not originate from low viscosity, but is rather determined by bilayered domain structure and specific molecular orientation of cations tails in the shear flow. The [C14mim][PF6] has a very unstable tribological behavior due to a narrow temperature range of its mesophase around 70°C and possible solid properties at this condition cannot be excluded. The [C14mim][Tf2N] has no mesophase, no specific orientational order, and consequently no ultralow friction regime in sliding contacts seem to

occur.

5. Acknowledgment

We gratefully acknowledge the financial support from the Deutsche Forschungsgemeinschaft, DFG, within Priority Program No. SPP-1191.

REFERENCES

- [1] M.-D. Bermúdez, A.-E. Jiménez, J. Sanes and F.-J. Carrión, *Molecules*, vol. 14, pp. 2888-2908, 2009.
- [2] I. Minami, *Molecules*, vol. 14, pp. 2286-2305, 2009.
- [3] P. Wasserscheid and T. Welton, 2 ed., P. Wasserscheid and T. Welton, Eds., Wiley-VCH, Weinheim, 2007.
- [4] R. D. Rogers and K. R. Seddon, 1 ed., American Chemical Society, 2005.
- [5] R. Hayes, S. Z. El and R. Atkin, *J. Phys. Chem. B*, vol. 113, pp. 7049-7052, 2009.
- [6] D. Wakeham, R. Hayes, G. G. Warr and R. Atkin, *The Journal of Physical Chemistry B*, vol. 113, pp. 5961-5966, 2009.
- [7] N. Pogodina, M. Nowak, J. Läger, C. Klein, M. Wilhem and C. Friedrich, *Journal of Rheology*, vol. 55, pp. 241-256, 2011.
- [8] N. V. Pogodina, E. Metwalli, P. Müller-Buschbaum, K. Wendler, R. Lungwitz, S. Spange, J. L. Shamshina, R. D. Rogers and C. Friedrich, *The Journal of Physical Chemistry Letters*, vol. 2, p. 257, 2011.
- [9] T. Amann, C. Dold and A. Kailer, *Soft Matter*, vol. 8(38), pp. 9840-9846, 2012.
- [10] T. Amann, C. Dold and A. Kailer, <http://dx.doi.org/10.1016/j.triboint.2013.03.021i>, 2013.
- [11] C. Dold, T. Amann and A. Kailer, *Lubr. Sci.*, vol. 25, pp. 251-268, 2013.
- [12] M. Walter, T. Amann, K. Li, A. Kailer, J. Rühle and M. Moseler, DOI: 10.1021/jp400980y, 2013.
- [13] K. Li, T. Amann, M. Walter, M. Moseler, A. Kailer and J. Rühle, DOI: 10.1021/la400333d, 2013.
- [14] R. K. Seddon, A. Stark and M.-J. Torres, in *ACS Symposium Series*, vol. 819, American Chemical Society, 2002, pp. 34-49.
- [15] S. Cuadrado-Prado, M. Dominguez-Perez, E. Rilo, S. Garcia-Garabal, L. Segade, C. Franjo and O. Cabeza, *Fluid Phase Equilibria*, vol. 278, pp. 36-40, 2009.
- [16] T. Itoh, N. Watanabe, K. Inada, A. Ishioka, S. Hayase, M. Kawatsura, I. Minami and S. Mori, *Chemistry Letters*, vol. 38, pp. 64-65, 2009.
- [17] K. Binnemans, *Chemical Reviews*, vol. 105, pp. 4148-4204, 2005.
- [18] K. V. Axenov and S. Laschat, *Materials*, vol. 4, pp. 206-259, 2011.
- [19] K. Goossens, K. Lava, P. Nockemann, K. V. Hecke, L. V. Meervelt, P. Pattison, K. Binnemans and T. Cardinaels, *Langmuir*, vol. 25, pp. 5881-5897, 2009.
- [20] T. Amann and A. Kailer, *Wear, Special Issue 18th International Conference on Wear of Materials*, vol. 271, pp. 1701-1706, 2011.
- [21] T. Amann and A. Kailer, *Tribology Letters*, vol. 41, no. 1, pp. 121-129, 2011.
- [22] T. Amann and A. Kailer, *Tribology Letters*, vol. 37, no. 2, pp. 343-352, 2010.
- [23] X. Wang, F. W. Heinemann, M. Yang, B. U. Melcher, M. Fekete, A.-V. Mudring, P. Wasserscheid and K. Meyer, *Chem. Commun.*, pp. 7405-7407, 2009.
- [24] P. Iglesias, M. Bermúdez, F. Carrión and G. Martínez-Nicolás, *Wear*, vol. 256, pp. 386-392, 2004.
- [25] A. H. Battez, R. González, J. Viesca, D. Blanco, E. Asedegbega and A. Osorio, *Wear*, vol. 266, pp. 1224-1228, 2009.
- [26] A. Jiménez, M. Bermúdez, F. Carrión and G. Martínez-Nicolás, *Wear*, vol. 261, pp. 347-359, 2006.
- [27] A. Jiménez, M. Bermúdez, P. Iglesias, F. Carrión and G. Martínez-Nicolás, *Wear*, vol. 260, pp. 766-782, 2006.
- [28] H. Kamimura, T. Kubo, I. Minami and S. Mori, *Tribology International*, vol. 40, pp. 620-625, 2007.

- [29] J. Qu, D. G. Bansal, B. Yu, J. Y. Howe, H. Luo, S. Dai, H. Li, P. J. Blau, B. G. Bunting, G. Mordukhovich and D. J. Smolenski, *ACS Appl. Mater. Interfaces*, vol. 4, pp. 997-1002, 2012.
- [30] C. Zhang, S. Zhang, L. Yu, P. Zhang, Z. Zhang and Z. Wu, *Tribology Letters*, pp. 1-6.
- [31] J. Qu, P. Blau, S. Dai, H. Luo and H. Meyer, *Tribology Letters*, vol. 35, no. 3, pp. 181-189, 2009.
- [32] S. Bulut, P. Klose and I. Krossing, *Dalton Trans*, vol. 40, p. 8114 – 8124, 2011.
- [33] J. De Roche, C. Gordon, C. Imrie, M. Ingram, A. Kennedy, F. Celso and A. Triolo, *Chem. Mater.*, vol. 15, p. 3089 – 3097, 2003.
- [34] C. Tanford, *J. Phys. Chem.*, vol. 76, pp. 3020-3024, 1972.
- [35] C. Li and J. He, *Colloid Interface Sci.*, vol. 359, pp. 474-480, 2011.
- [36] R. G. Larson, 1 ed., Oxford Univ Pr, 1998, p. 509.
- [37] G. G. Fuller, *Optical Rheometry of Complex Fluids*, Oxford University Press: Oxford, 1995.
- [38] G. G. Fuller, *Rheology Reviews*, p. 77 – 123, 2003.